Microchimica Acta (2023) 190:112
https://doi.org/10.1007/s00604-023-05687-1

ORIGINAL PAPER

Self-assembled monolayer-assisted label-free electrochemical genosensor for specific point-of-care determination of *Haemophilus influenzae*

Hessamaddin Sohrabi[1] · Mir Reza Majidi[1] · Karim Asadpour-Zeynali[1,2] · Alireza Khataee[3,4] · Ahad Mokhtarzadeh[5]

Received: 2 November 2022 / Accepted: 31 January 2023 / Published online: 4 March 2023

Abstract

For sensitive detection of the *L-fuculokinase* genome related to the *Haemophilus influenzae* (*H. influenzae*), this research work demonstrates the label-free electrochemical-based oligonucleotide genosensing assay relying on the performing hybridization process. To enhance the electrochemical responses, multiple electrochemical modifier-tagged agents were effectively utilized. For attaining this goal, NiCr-layered double hydroxide (NiCr LDH) has been synthesized and combined with biochar (BC) to create an efficient electrochemical signal amplifier that has been immobilized on the surface of the bare Au electrode. Low detection and quantification limits (LOD and LOQ) associated with the designed genosensing bio-platform to detect *L-fuculokinase* have been achieved to 6.14 fM and 11 fM, respectively. Moreover, the wide linear range of 0.1 to 1000 pM demonstrates the capability of the designed platform. Investigated were the 1-, 2-, and 3-base mismatched sequences, and the negative control samples clarified the high selectivity and better performance of the engineered assay. The values of 96.6–104% and 2.3–3.4% have been obtained for the recoveries and RSDs, respectively. Furthermore, the repeatability and reproducibility of the associated bio-assay have been studied. Consequently, the novel method is appropriate for rapidly and quantitatively detecting *H. influenzae*, and is considered a better candidate for advanced tests on biological samples such as urine samples.

Keywords *Haemophilus influenzae* · NiCr LDH · Biochar · AuNP genosensor · DNA hybridization · Differential-pulse voltammetry

Introduction

Haemophilus influenzae is a gram-negative coccobacillus bacterium classified by generating polysaccharide capsules found in human respiratory tracks. It is a commensal in the human nasopharynx, mostly existing on the mucosal surfaces. This pathogenic agent results in, for instance, meningitis and pneumonia, and in the bloodstream, epiglottitis, infections, and septicemia. Based on the presence or absence of a tough polysaccharide capsule, *H. influenzae* is divided into encapsulated (six serotypes, a–f) and non-encapsulated strains. Being resistant to the phagocytosis and complement system is provided by the capsule; hence, non-capsulated strains contain less invasive attributes. Therefore, *H. influenzae* can be considered the desired target for the development of novel detection systems as well as vaccine development. Consequently, sensitive and rapid recognition of *H. influenzae* is considered in medical microbiology [1–4].

✉ Mir Reza Majidi
majidi@tabrizu.ac.ir; sr.majidi@gmail.com

✉ Ahad Mokhtarzadeh
mokhtarzadehah@tbzmed.ac.ir

[1] Department of Analytical Chemistry, Faculty of Chemistry, University of Tabriz, Tabriz 51666 16471, Iran

[2] Pharmaceutical Analysis Research Center and Faculty of Pharmacy, Tabriz University of Medical Sciences, Tabriz, Iran

[3] Research Laboratory of Advanced Water and Wastewater Treatment Processes, Department of Applied Chemistry, Faculty of Chemistry, University of Tabriz, Tabriz 51666-16471, Iran

[4] Department of Environmental Engineering, Gebze Technical University, 41400 Gebze, Turkey

[5] Immunology Research Center, Tabriz University of Medical Sciences, Tabriz, Iran

The currently introduced methods for the determination of *H. influenzae* are mostly molecular approaches, such as PCR (polymerase chain reaction)-based methods [5], immunochromatography [6], culture-based phenotypic identification [7], immunoglobulin analysis [8], serotyping by agglutination including LAT (latex particle agglutination) [9], and capsular genotyping [10]. Some drawbacks considered of these approaches are low sensitivity and specificity, time-consuming, laboriousness, and the requirement of developed expensive instruments and expert technicians [11–13]. Nevertheless, because of being a fastidious bacterium, growing this kind of bacterium species requires complex nutrition [14]. Furthermore, replicating such species is laborious and time-consuming, and several days or weeks are sometimes needed [15–18]. Due to the constraints of common methods concerning biological molecule detection (particularly *H. influenzae*), biosensing platforms were used for more sensitive and specific detection of *H. influenzae* [19–22].

Because of high selectivity and the low cost of detected analytes [23–28] and the miniaturization possibility [29–32], electrochemical biosensors (EBs) [29, 33–37] are encouraging tools for the detection of *H. influenzae*. Electrochemical devices [38–41] integrate a biological recognition element, including proteins, nucleic acids, and antibodies that have selective reactions with the analyte [30, 34, 42–44]. Recently, DNA-based platforms were extensively used for detection aims due to their minimization ability, simplicity, low cost, specificity, and great sensitivity. DNA hybridization is the main process in fabricating DNA-based sensing assays in which ss-pDNA (single-stranded probe DNA) can be applied for immobilizing on the modified electrode, and ss-tDNA (single-stranded target DNA) can bind to it to form the double-stranded helix (ds-DNA). With the emergence of nanotechnology, different nanoparticles are used for immobilizing thiolated DNA probes with outstanding attributes such as electrochemical and optical modifier agents, biocompatibility, great surface area, and great adsorption capability [45–49].

Layered double hydroxides (LDHs) [19] as host–guest layered compounds consist of positively charged metal hydroxide layers with anions trapped within interlayer galleries [50] and can be considered nanostructures with two dimensions that contain special chemical and physical characteristics [51]. LDHs can be synthesized utilizing different approaches such as sol–gel, electrodeposition, co-precipitation hydrothermal, and urea hydrolysis methods. These two-dimensional compounds attracted much attention because of their special characteristics like tunable characterization, water-resistant structures, high anion exchange capacities, ease of preparation, low cost, high surface area, non-toxicity, layered composition, and antacids. LDHs can be greatly utilized in analytical extractions [52], adsorption [53], drug delivery [54], flame retardants [55], fuel cells [56], and catalysis [57–59], as well as their important usage in biosensing and sensing assays. On the other hand, biochar (BC), as a modifier agent, has gained too much attention in this capacity. BC can be considered as the carbon-rich material achieved by heating biomass, like wood, manure, or leaves in a closed container with little or no available air. Some significant benefits of BC include high surface area, sustainability, cost-effectiveness, unequaled porous structure, and a simple production process permitting the facile synthesis of carbon-based nanocomposites [42, 60–62]. Nevertheless, utilizing greatly conductive BC-derived nanocomposites for constructing electrochemical-based genosensing assays has not been widely investigated. Additionally, gold nanoparticles (AuNPs), as conductive mediators, can be used to enhance the electrical response and are also capable of maintaining biological activity. Therefore, AuNPs can be applied for the immobilization of DNA probes on the electrode surface [63, 64].

In the present paper, a new genosensing platform based on NiCr LDHs decorated with honeycomb-like BC (NiCr LDH@BC) was designed. The facile co-precipitation route was used to synthesize NiCr LDHs. In the following, the effective NiCr LDH@BC synthesis has been provided and consequently utilized as a capable modifier agent for modifying the Au electrode surface. The novelty of our research work is to develop a new label-free genosensing assay based on DNA hybridization and bioconjugation for determining *H. influenzae* in urine samples by applying the newly synthesized nanocomposite. Long-term stability, high sensitivity, and simple design are the most dominant analytical features of the introduced genosensor in comparison with similar research works.

Materials and methods

Chemical agents

Sodium hydroxide pellets (NaOH), nickel (II) nitrate hexahydrate ($Ni(NO_3)_2{\cdot}6H_2O$), chromium (III) nitrate nonahydrate ($Cr(NO_3)_3.9H_2O$), DL-Dithiothreitol (DTT), hydrogen peroxide solution (H_2O_2, 30%), acetone (CH_3COCH_3), hydrochloric acid (HCl), sulfuric acid (H_2SO_4), sodium acetate (CH_3COONa), mercaptoethanol ($HS(CH_2)_6OH$), ammonia solution (NH_3, 25%), and ethanol were obtained from Merck (Germany). Biochar was formed through the pyrolysis of pine trees (*Pinus halepensis*) using a curtain flame. Hydrogen tetrachloroaurate (III) hydrate ($HAuCL_4{\cdot}3H_2O$), potassium ferrocyanide $K_4Fe(CN)_6$, potassium ferricyanide $K_3Fe(CN)_6$, and potassium chloride (KCl) were obtained from Sigma-Aldrich Co.

Apparatus and instrumentation

The Potentiostat/Galvanostat Autolab PGSTAT 30 (Eco Chemie B.V., The Netherlands) was applied for performing the electrochemical and biosensing analyses. The

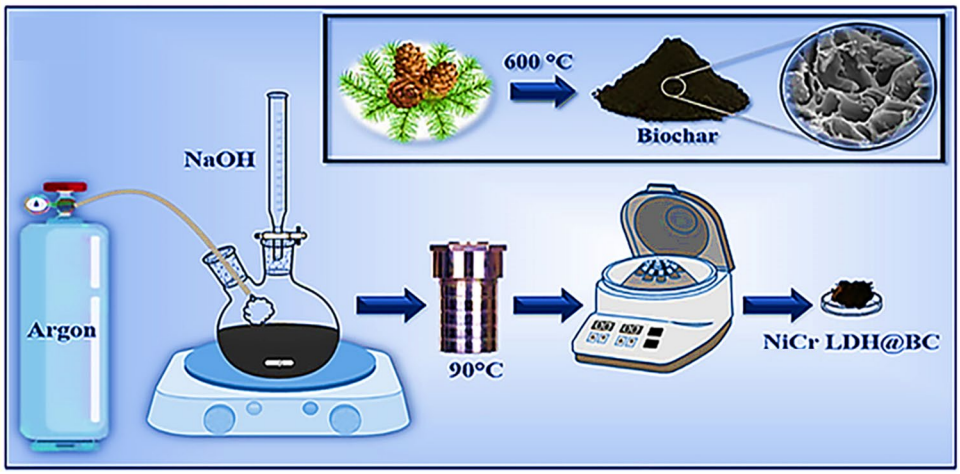

Scheme 1 Fabrication process NiCr LDH, BC, and the NiCr LDH@BC nanocomposite

electrochemical analysis was performed in a cell containing three electrodes. The bare and also modified gold (Au) electrodes were used as working electrodes ($d = 2$ mm). The auxiliary electrode was a Pt wire electrode and the reference electrode was a saturated calomel electrode (SCE, Hg_2Cl_2) in KCl solution. All electrodes were purchased from Azar Electrode Co. (Urmia, Iran). For characterization purposes, the Fourier transform infrared (FT-IR) spectra were obtained from Bruker Instruments, Germany, model Aquinox 55. For explaining the morphology of the surface, scanning electron microscopy (SEM) was investigated on a MIRA3 FEG-SEM TESCAN made in the Czech Republic. HRTEM (Thermo ScientificTM Talos F200S 200 kV S, USA) was used to control the morphology of the fabricated compounds. The composition of synthesized NiCr LDH and NiCr LDH@BC by X-ray diffraction (XRD) analysis was examined by Siemens diffractometer (D500 S) at room temperature applying the scan range of 2θ from 5 to 70° and Cu-Kα radiation at 35 kV.

The synthesis steps of the modifier agent

Preparation of biochar

Biochar was fabricated from pine tree (*Pinus halepensis*) residues by applying a pyrolysis process using a flame curtain kiln. This kind of kiln is a conical metal container that lets the biomass get pyrolyzed layer by layer. The pyrolysis process was performed for 1 h at about 600 °C. The provided biochar was quenched with water and after drying in the air for 4 days, it was ground and passed from a 2-mm sieve to produce a product with uniform particle size.

The synthesis of NiCr LDH nanosheets

The facile co-precipitation route was utilized to synthesize NiCr LDH. Initially, 4.57 and 5.81 g of $Cr(NO_3)_3{\cdot}9H_2O$ and $Ni(NO_3)_2{\cdot}6H2O$ were dissolved in distilled water, respectively. NaOH solution (1 mol L^{-1}) was added drop by drop, along with the maintaining solution under argon gas, and magnetically stirred to achieve a pH of 8.5–9. Subsequently, the obtained suspension was further stirred for 24 h at 65 °C. Eventually, the obtained NiCr LDH was retrieved by centrifuge and dried at 60 °C in the oven. Scheme 1 demonstrates the schematic of the synthesis method applied in this study.

The synthesis of NiCr LDH@BC

To synthesize NiCr LDH@BC, 0.08 g of BC solution was dispersed ultrasonically in 10 mL distilled water. NaOH solution (2 mol·L^{-1}) was added to the $Cr(NO_3)_3{\cdot}9H_2O$ and $Ni(NO_3)_2{\cdot}6H_2O$ solutions and the pH was raised to 9. Then, the solution was mixed with the ultrasonicated BC solution and stirred for an extra 30 min, and transferred into a stainless-steel autoclave. The autoclave was placed in the oven at 90 °C for 24 h. The generated precipitate was rinsed with distilled water and dried at 60 °C for 18 h (Scheme 1).

Designing the electrochemical genosensing bio-assay

In this regard, ss-pDNA has been mixed with DTT to prepare an appropriate and active probe sequence. DTT can be used as an efficient protecting intermediary for SH- functional groups in ss-pDNA probes and inhibits the oxidation of the thiol group. The sulfur atoms of the thiolated ends want to dimerize in the presence of molecular oxygen. The impact of the electrode modifier agents on Au electrodes in biosensing assays can greatly be reduced by the formation of dimer compounds. In this study, a 10-µL DTT has been added to a 10-µL ss-pDNA solution. Subsequently, a vortex has been applied to combine the obtained solution, and later, it has been placed at 25 °C for 30 min. Eventually, for obtaining NiCr LDH/BC/AuNPs/ss-pDNA/Au electrodes, the solution has been cast on the surface

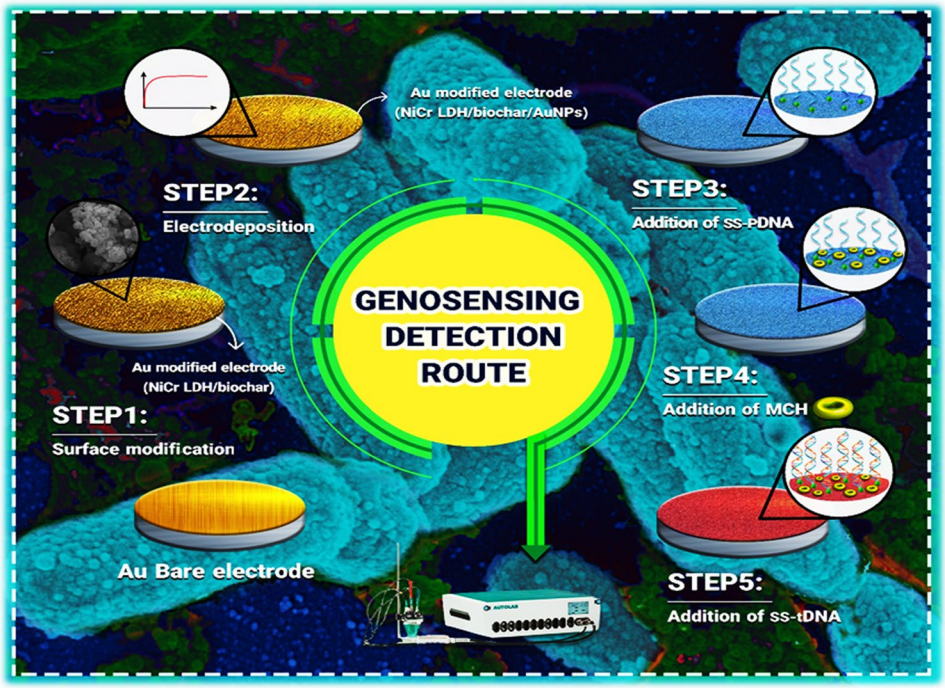

Scheme 2 Schematic illustration of the designed bio-assay for highly sensitive recognition of *H. influenzae*

of the modified Au electrodes and incubated for 5 h at 4 °C. At this stage, the modified Au electrode has been incubated by MCH at 25 °C for 30 min. MCH is capable of displacing the non-specific interactions between AuNPs and the DNA and forming a self-assembled monolayer (SAM), which can resist the nonspecific ss-tDNA adsorption. Blocking the non-reacted AuNPs with DNA probe is the critical point. In addition, MCH can significantly enhance the ss-tDNA immobilization capability at the next step. Blocking effectively the unresponsive sites is obtained by MCH. Filling the remaining Au locations and producing a well-organized assay are obtained by MCH immobilization. Eventually, for applying the hybridization process at 37 °C, the ss-tDNA has been cast on the Au-modified electrode surface. Scheme 2 highlighted the performance of the proposed gene detection assay.

Results and discussion

Characterization of NiCr LDH and NiCr LDH@BC

Morphological investigations (SEM and TEM)

SEM analysis was applied to assess the morphology characterization of the NiCr LDH and its BC-based nanocomposite (Fig. 1B and C). The NiCr LDH has a layered crystal structure with firmly stacked layers, as can be observed. Similar morphology was reported for NiCr LDH in the previous works [65, 66]. Additionally, regarding the modified electrodes, SEM images of Au bare electrodes are shown in Fig. 2A. After modification of the electrode surface with NiCr LDH (Fig. 2B and C), the presence of layered crystal structures confirms the successful immobilization of the synthesized NiCr LDH on the surface of the Au electrode. On the other hand, Fig. 2D–F depict the Au electrode modification with NiCr LDH@BC composite. Likewise, the existence of NiCr LDH inside the pores and on the surface of the BC can be well asserted. It is significant to mention that various characterization information regarding BC have been reported in our previous research work [67].

Further investigation on the morphology of the so-prepared samples was carried out by TEM analysis. The sheets of the NiCr LDH can be seen in Fig. 1C, approving the layered structure of the NiCr LDH. Furthermore, the presence of the layered structure of NiCr LDH on the BC can be seen in Fig. 1D.

Investigation of the various functional groups

The FT-IR spectra of the NiCr LDH and NiCr LDH@BC samples are illustrated in Fig. 1E. Based on the literature review, the FT-IR spectrum of the so-synthesized samples can be approximately described as follows: (1) the O–M–O vibration associated with the LDH layer causes the absorption peaks at 450–550 cm^{-1}; (2) the Ni–O and Cr–O vibration is responsible for the absorption < 1000 cm^{-1}; (3) the stretching vibration of NO_3^- causes the absorption at 1384 cm^{-1}; (4) the absorption at 1630 cm^{-1} comes from the bending vibration of H–O–H; (5) the peak located in 2950 cm^{-1} is associated with the stretching absorbance of C–H; (6) the stretching mode of the OH group in the LDH layer and the adsorbed water caused the wide absorption peak at 3440 cm^{-1}.

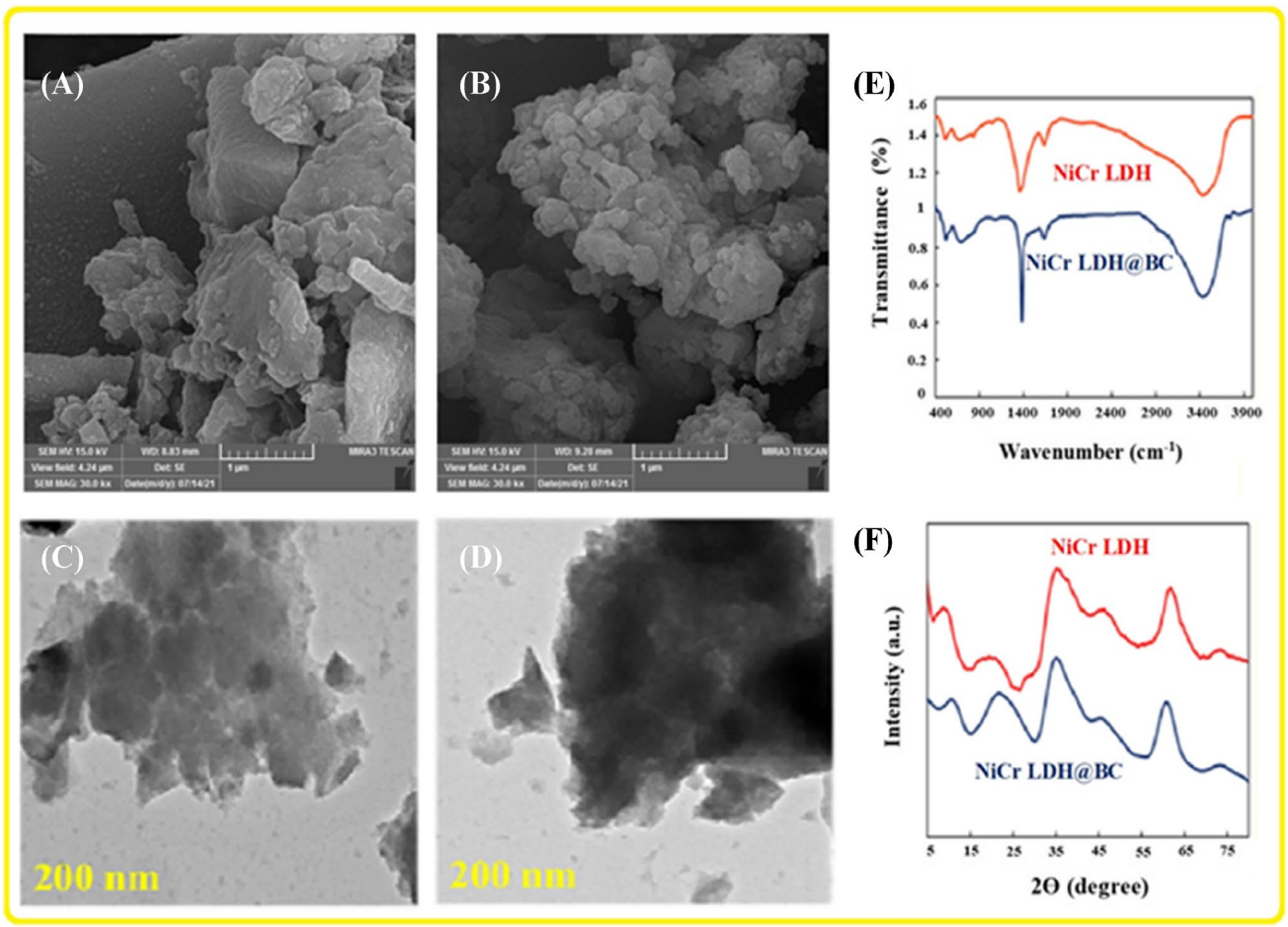

Fig. 1 SEM images of NiCr LDH (**A**) and NiCr LDH@BC (**B**), FT-IR spectra of NiCr LDH and NiCr LDH@BC (**C**), TEM images of NiCr LDH (**D**) and NiCr LDH@BC (**E**), XRD patterns of NiCr LDH and NiCr LDH@BC (**F**)

XRD patterns

The XRD spectra of the as-prepared catalysts are depicted in Fig. 1F. XRD pattern of NiCr LDH and NiCr LDH@BC fitted well by the existence of diffraction peaks at (003), (006), (012), (015), (018), (110), and (113) (JCPDS PDF- 96–210-2794) [68]. The XRD patterns validated the successful synthesis of NiCr LDH and NiCr LDH@BC. The characteristic bands of BC were not observed in the XRD patterns owing to the low amount of BC in the nanocomposite structure.

Electrochemical properties of the designed genosensor

Electrochemical feasibility

The voltammograms in a $[Fe(CN)_6]^{3-/4-}$ the solution were used to evaluate the electrochemical behavior related to changes in the Au electrode via the process of modification. Figure 3A represents the achieved electrochemical voltammograms concerning Au bare electrode, Au-modified electrode by NiCr LDH sheets, and NiCr LDH@BC. Furthermore, the chronoamperometry (ChA) method is used for carrying out the electrodeposition of AuNPs on a modified Au electrode (NiCr LDH@BC/AuNPs/Au electrode). Accordingly, the Au electrode was effectively modified by ss-pDNA (NiCr LDH@BC/AuNPs/ss-pDNA/Au electrode), and ss-tDNA (NiCr LDH @BC/AuNPs/ss-pDNA/ss-tDNA/Au electrode) represents different electrochemical responses, which demonstrates the effective hybridization process. A peak current of 21.8 µA at 0.25 V is represented for the achieved voltammograms concerning a bare Au electrode. After Au electrode surface modification via the immobilization of NiCr LDH, the peak current of oxidation is enhanced and the potential reduced as well which represents the suitability of NiCr LDH sheets as an efficient modifier for fabricating the electrochemical sensing platform (66.4 µA in 0.215 V). The peak current increased to 126 µA (0.244 V) after immobilization of NiCr LDH@BC on the Au electrode surface. According to what was obtained from the CVs, the presence of BC and NiCr LDH enhanced the peak current. The electrode surface area and

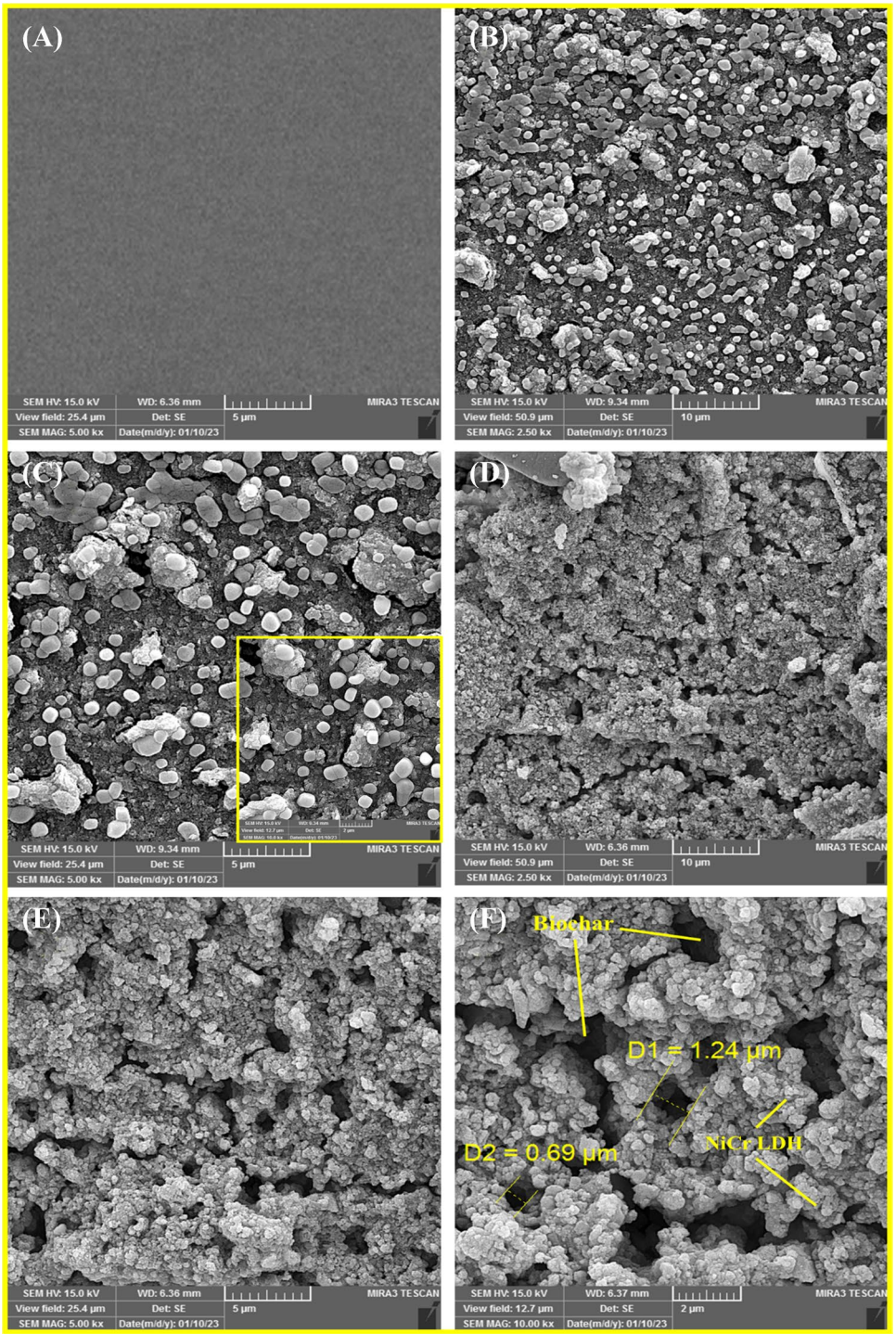

Fig. 2 SEM images of Au electrode: Au bare electrode (**A**), Au-modified electrode with NiCr LDH (**B** and **C**), Au-modified electrode with NiCr LDH@BC (**D**–**F**) in various magnifications

the electron transfer rate can be improved by applying the BC and NiCr LDH. Subsequently, electrodeposition of the AuNPs as the final modification stage has been performed on the Au electrode surface. This modification step leads to an upsurge in the peak current (152 µA at 0.239 V) that has been presented in Fig. 3A. The use of AuNPs can afford an appropriate surface for the immobilization of the thiolated ss-pDNA and improve the efficiency of the electrochemical reaction in the considered sensing platform. A small reduction in currents has been noted in the oxidation peak after immobilizing ss-pDNA. Such alterations are associated with the strong S–Au bounds among thiolated ss-pDNA and AuNPs. At the final stage, ss-tDNA has been dropped on the surface of the Au electrode and hybridization happened after fabricating the gene-sensing bioassay, where the peak current has been reduced to 86.2 µA.

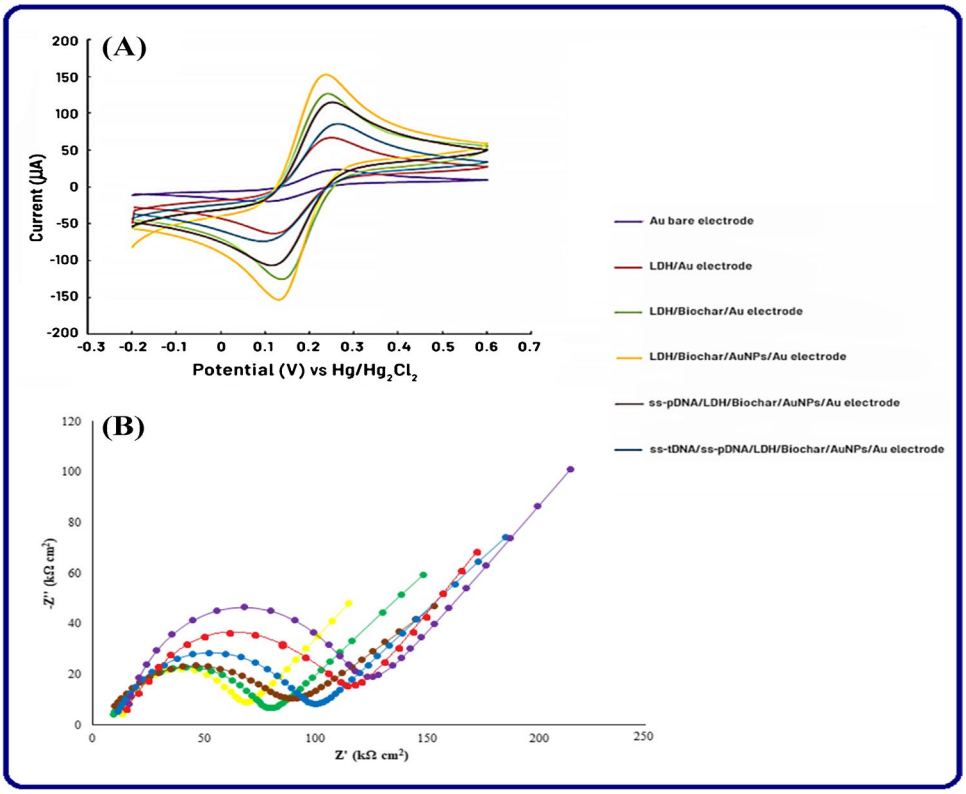

Fig. 3 The electrochemical investigation: CV of the proposed assay (**A**), EIS Nyquist plots (inset: Randles circuit) (**B**) for determination of the *L-fuculokinase* genome based on NiCr-layered double hydroxides (LDHs)/BC/AuNP nanocomposite

Electrochemical impedance spectroscopy (EIS)

Electrochemical impedance spectroscopy represents the different changes in the obtained electrochemical signals due to the modifications of the surface of the working electrode on the interfacial electron-transfer resistance (Ret). The acquired impedimetric values can also be depicted as Nyquist plots which consist of two significant parts: (1) a semicircle shape in the higher frequency range and (2) a straight line in the lower frequency range. The appropriate data fitting process for providing the associated impedance spectra considers a significant part of EIS-based analysis. To achieve this purpose, the Randles circuit in its modified form is professionally used in the various series of data for performing the fitting process. Charge-transfer resistance (*R*ct), solution resistance (*R*s), Warburg impedance (*Z*w), and constant phase element (CPE) are four significant parameters of the Randles circuit. Figure 3B reveals the impedance curves associated with the various modification steps of the Au electrode which were recorded in the $[Fe(CN)_6]^{3-/4-}$ solution as a redox probe at the potential of 0.25 V which the constant frequency ranges from 100 kHz to 10 MHz. Between these parameters, the Rct values of the Au electrode were recorded for each modification step. As provided, the modification of the electrode surface influences the kinetics of electron transfer. As clear from the obtained results, the charge-transfer resistance related to the unmodified Au electrode is expressively larger than the modification steps and also confirms the diffusion-controlled process of the electrochemical reaction of the redox probe. In addition, the order of Rct values for each modification step should be considered. NiCr LDH/Au electrode > NiCr LDH@BC/Au electrode > NiCr LDH@BC/AuNPs/Au electrode. The obtained results meaningfully confirm that the low Rct value for NiCr LDH@BC/AuNPs/Au electrode, in comparison with the unmodified Au electrode, might have occurred due to layered structure features and the ion exchange process. On the other hand, the lessening tendency of the Rct amounts in the NiCr LDH/Au electrode, NiCr LDH@BC/Au electrode, and NiCr LDH@BC/AuNPs/Au electrode exposes that the presence of NiCr LDH, BC, and AuNPs as effective modifiers of Au electrode results in the acceleration of the electron transfer rate and providing a larger surface area. Moreover, the obtained EIS results powerfully approve that the fabricated NiCr LDH@BC nanocomposite owns good conductivity which considerably eases electron transfer more effectively on the surface of an Au-modified electrode. As clearly depicted in Fig. 3A and B, the acquired outcomes of the EIS technique are compatible with those of CVs in which the superlative electrochemical response belongs to the NiCr LDH@BC/AuNPs/Au electrode. Through dropping of ss-pDNA on the NiCr LDH@BC/AuNPs/Au electrode,

an increase in the Rct value has occurred due to the accumulation of more electrostatic repulsive forces between the electro-negative phosphate group in DNA and the negatively charged redox species which finally prevents the effective movement of $[Fe(CN)_6]^{3-/4-}$ ions during a redox reaction. At the final stage, by casting ss-tDNA more increase in Rct values can be observed with is compatible with CV results.

Optimization steps

Concentration of the modifier agent

This optimization step represented the concentration effect of the modifier agent in the analytical response intensities. According to Fig. 4A and B, when the concentration increases from 1 to 5 mg·mL^{-1} the maximum current density is achieved in 5 mg·mL^{-1} for the LDH@BC-incorporated AuNPs/Au electrode along with increasing the peak current (ΔI = Iss-pDNA-Iss-tDNA). Thereafter, a significant decrease in electrochemical responses was observed in 6 and 7 mg·mL^{-1} of the prepared nanocomposite. This is probably because of a thick layer emerging on the modified gold electrode surface that decreases sensitivity by blocking the electron transfer pathways and avoiding reaching the surface of the electrode as well. Consequently, the appropriate concentration of the fabricated nanocomposite has been improved to 5 mg·mL^{-1}.

Volume of the modifier agent

Additionally, optimizing the volume of the modifier agent is a significant stage because of the effect on the efficiency of the designed sensing platform. For obtaining this aim, different quantities of NiCr LDH@BC composite including 2–10 µL of the modifier volume (5 mg mL^{-1}) have been investigated. According to the obtained findings, 6 µL of the presented mixture on the surface of the Au electrode

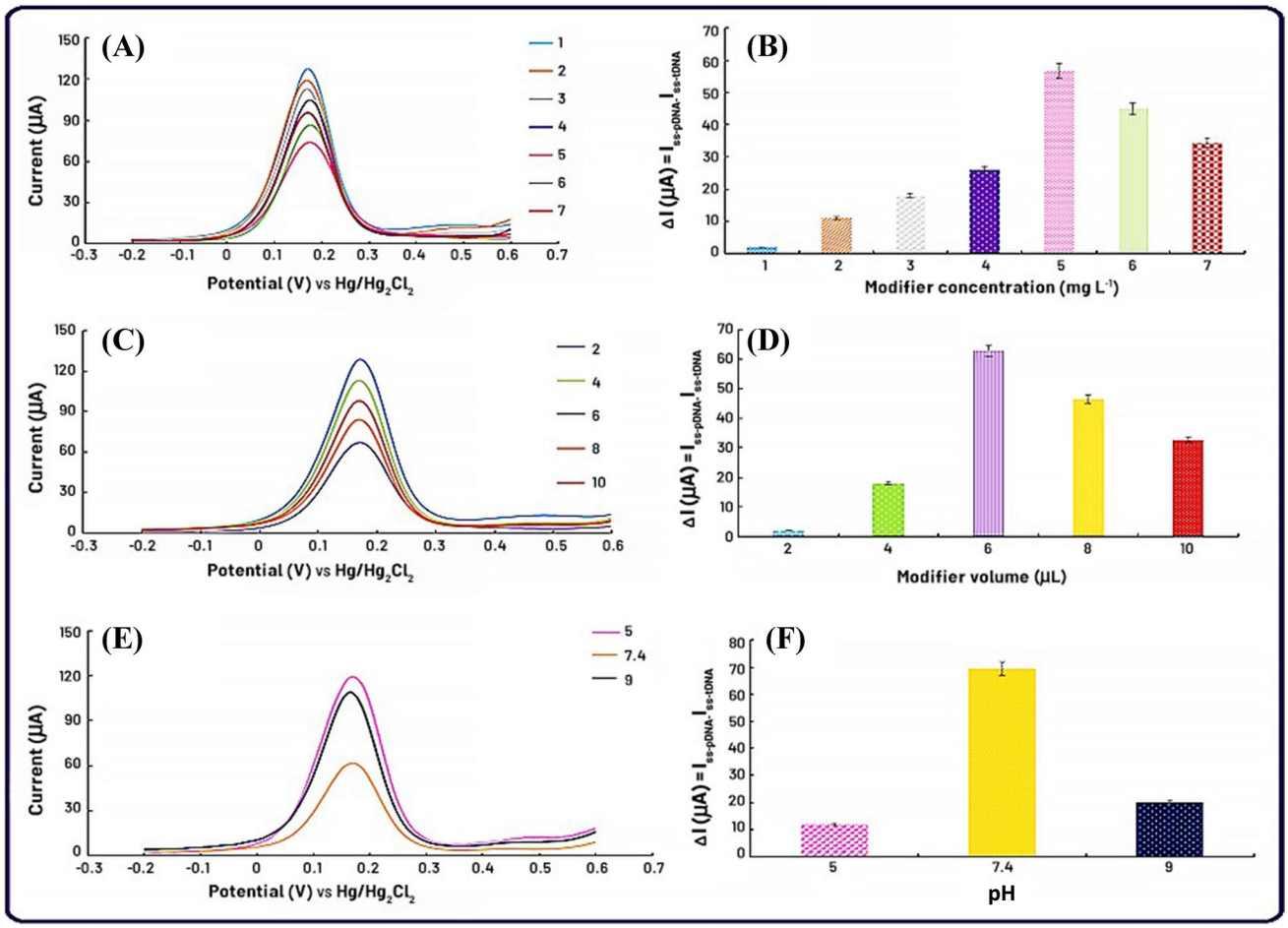

Fig. 4 Investigation of the various optimization steps representing modifier agent. The concentration effect related to the modifier agent (**A**). Histogram of the modifier concentration optimization (**B**). The volume of modifier agent (**C**). Histogram of the modifier volume optimization step (**D**). The effect of various pHs (acidic, neutral, and basic) on the performance of the designed modifier agent (**E**). Histogram related to the various applied pHs (**F**)

has to be the optimum volume. Subsequently, after 8 µL, a reduction in the electrochemical response may be due to the modifier agent compression which results in a decrease in peak currents (Fig. 4C and D).

The effect of applying various pH

At last, the effect of pH at basic, neutral, and acidic media (pH of 9, 7.4, and 5) was performed to reveal the dependence of pH on the performance of the designed assay. The outcomes of Fig. 4E and F represented the achievement of the best electrochemical signal at neutral pH. Acidic and basic pH can result in the denaturation of proteins and nucleic acids. The surface charge of biomolecules can be changed by the change of pH from neutral to acidic or basic and the changing tertiary or quaternary structure of biomolecules can be obtained by their intramolecular bonds, resulting in the ineffectiveness of the interactions and deformation of active sites. Hence, all experiments can have a suitable value of the normal physiological pH of 7.4.

ss-pDNA immobilization time

The ss-pDNA immobilization time contains a significant effect on the sensitivity of the designed gene-detection platform and better performance of the hybridization process. In this study, for obtaining the optimal time for the best performance of the designed biosensor, the ss-pDNA immobilization time has been investigated for 1–7 h. According to Fig. 5A and B, an increase of 1 to 5 h in the immobilization time can also increase the related peak current. Afterward, when the immobilization time steadily increases, the electrochemical response decreases as well. Accordingly, 5 h has been selected for the optimum immobilization time of ss-pDNA on the surface of the Au-modified electrode.

Hybridization time and temperature

According to Fig. 5C and D, hybridization time can effectively influence the genosensor efficiency. A decrease of 130 to 60 µA has been observed for the electrochemical signal whereas an increase of 10–50 min has been observed for the DNA hybridization time. Finally, the best hybridization time of the designed platform is considered to be 50 min. Additionally, several temperatures varying from 25 to 55 °C were used to investigate the impact of the hybridization temperature on the electrochemical responses of the $Fe(CN)_6^{3-/4-}$ redox probes. According to Fig. 5E and F, an increase from 25 to 37 °C and then a decrease is obtained for the signal. Such a decrease can happen because of the instability of the DNA probe and nucleotide at greater temperatures. Even though the best biosensor response has been obtained at 37 °C, other experiments have been performed at ambient temperature for avoiding the complications of using the biosensor.

Kinetic investigation

Figure 6 represents the associated voltammograms of the modified electrodes obtained at various scan rates. With the help of the CV approach, various scan rates of 10–300 mVs^{-1} are used to examine the kinetic performance of the designed platform. According to Fig. 6A, a progressive increase in the voltammogram width can be observed and the anodic and cathodic peaks increase significantly at higher scan rates. According to Fig. 6B, the linear dependence ($R^2 = 0.999$) of anodic peak currents with square roots of scan rates can be observed by the scan rate analysis. According to the results, the diffusion process can control the transfer of mass from the inside of the solution to the electrode surface. Therefore, the following Randles–Sevcik equation can be used to explain the electrochemical process:

$$Ip = 2.69 \times 10^5 A D^{1/2} n^{3/2} C \upsilon^{1/2} \quad (1)$$

In this equation, Ip represents the peak current, A represents the electroactive surface (cm^2), D represents the molecular diffusion coefficient of solution ($cm^2\ s^{-1}$), the electron transfer in the electrochemical reaction is represented by n, υ represents the scan rate ($V\ s^{-1}$), and C represents the concentration of the analyte ($mol\ dm^{-3}$).

On another hand, the linear dependence ($R^2 = 0.998$) of Ln Ip vs Ln υ in the selected scan rate range of 10–300 $mV\ s^{-1}$ is presented in Fig. 6C. For explaining the mass transfer mechanism, the slope is represented by Fig. 6C as 0.5 and the value represents that the electrochemical reaction considers being diffusional control. Consequently, Fig. 6D demonstrates the non-linear pattern of the dependence of Ip vs υ and confirms the non-linear relation between Ip vs υ. Our electrochemical reaction does not contain an adsorption dependence.

Calculating Au-modified electrode surface area

For calculating the surface area, the designated Randles–Sevcik (Eq. 1) has been utilized. Ip represents the anodic peak current, n is equal to 1 which is named the electron transfer, C_0 represents the $[Fe(CN)_6]^{3-/4-}$ concentration (1 mM), ν represents the scan rate, and D ($0.76 \times 10^{-5}\ cm^2\ s^{-1}$) demonstrates the diffusion coefficient. According to the slope of Ip (µA) vs. υ ½ ($V^{1/2} \cdot s^{-1/2}$), 0.081 cm^2 has been estimated for the surface area of the

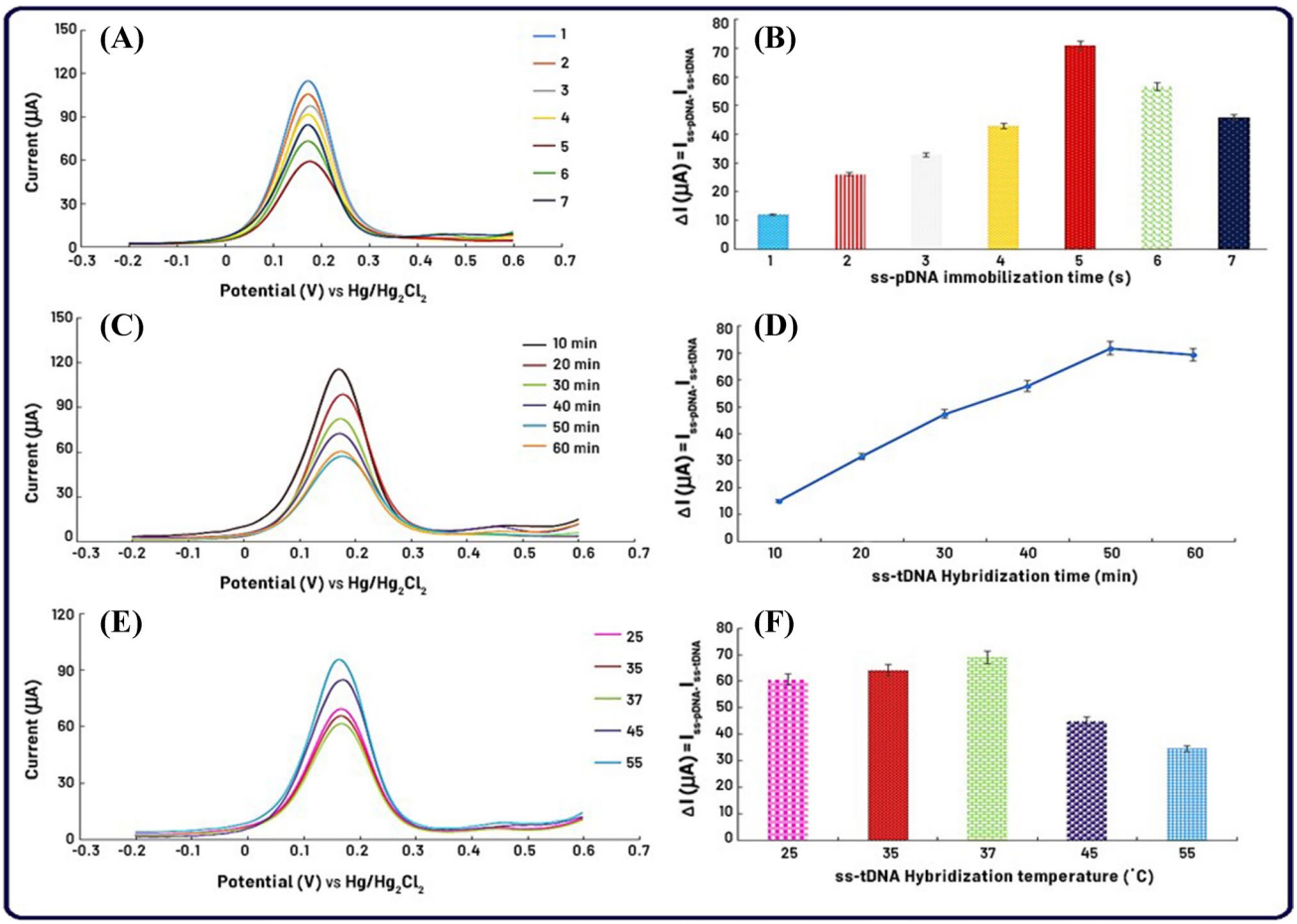

Fig. 5 DPVs of ss-pDNA immobilization time (1–7 h) on the surface of the Au electrode (**A**). Histogram of ss-pDNA immobilization time (**B**). Voltammograms of the hybridization process (10–60 min) (**C**). Histogram of the various immobilization time of ss-tDNA optimization (**D**). The effect of various temperatures associated with the hybridization process on the performance of the proposed sensing assay (**E**). Related histogram demonstrates the effect of various temperatures (**F**)

Au-modified electrode. According to the CV diagrams in Fig. 3, the increase in peak currents can be attributed to the increase in the surface of the modified electrode. The rest of the electrodes have an increase in surface area compared to the bare electrode, but the increase in surface area of the desired electrode is greater than the others. The order of the electrode surface areas associated with their CV voltammograms is as follows: NiCr LDH@BC/AuNPs/Au electrode > NiCr LDH@BC/Au electrode > NiCr LDH/Au electrode.

Calibration plot and investigation of the analytical features

When calculating the performance of a DNA-based genosensing assay, sensitivity is a significant parameter. Using the aforementioned optimum conditions, different concentrations of *H. influenzae* ss-tDNA are used to evaluate the genosensor performance. Figure 7 represents the values associated with DPVs of various ss-tDNA concentrations (0.1 pM, 1 pM, 10 pM, 25 pM, 50 pM, 75 pM, 100 pM, 250 pM, 1 nM). The achieved outcomes demonstrated that the increase of the ss-tDNA concentration could decrease the peak current. Because of the negative charge for DNA and $[Fe(CN)_6]^{3-/4-}$, a reduction in the current has ensued. Consequently, when recording the electrochemical signal by $Fe(CN)_6^{3-/4-}$, it is possible to recognize the occurrence or non-occurrence of the hybridization process. Considerably, the logarithm values of DPV peak currents and *H. influenzae* ss-tDNA concentration can present a suitable linear relation (Fig. 7B). According to the optimal conditions, R^2, LOD, LOQ, linear range (LR), and sensitivity were equal to 0.9991, 6.14 fM, 11 fM, 0.01–1000 pM, and 160.69 μA M^{-1} cm^{-2} respectively. When utilizing the fabricated genosensing bio-assay, *H. influenzae* can have great sensitivity. Furthermore, relative standard deviations (RSD%) of the tests have been obtained at 2.3–3.5.

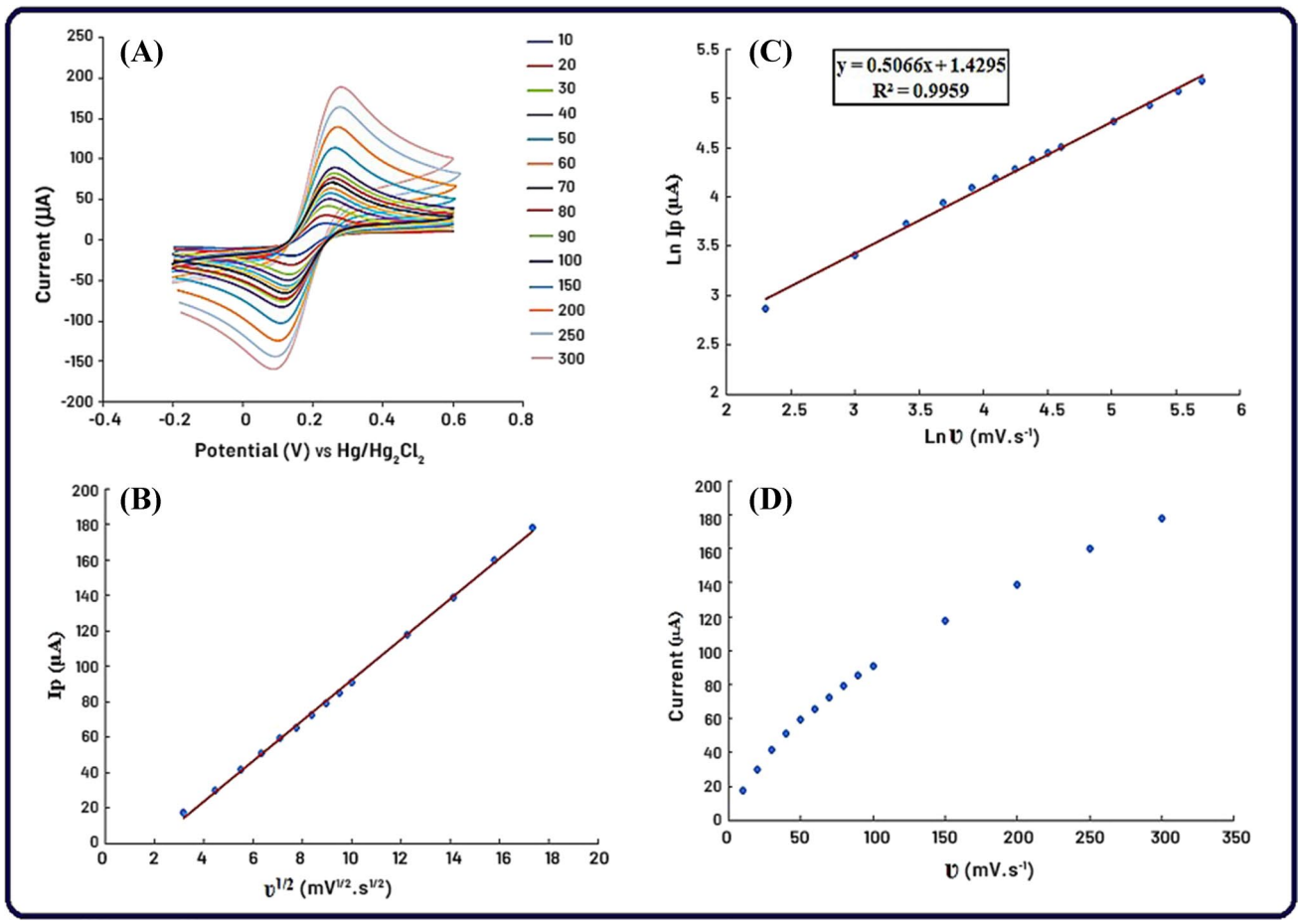

Fig. 6 CV voltammograms (**A**) of MoS_2/Biochar/AuNPs stabilized on the gold electrode in the solution of $Fe(CN)_6^{3-/4-}$ and KCl in different scan rates (1, 5, 10, 20, 30, 40, 50, 60, 70, 90, 100, 150, 200, 250, 300 mVs^{-1}): 0.01 M $[Fe(CN)_6]^{3-/4-}$ and 0.1 M KCl are applied as a supporting electrolyte, ss-pDNA concentration is 1 µM. Plot of Ip (µA) vs υ ½ ($V^{1/2}{\cdot}s^{-1/2}$) (**B**), Ln Ip (µA) vs Ln υ ($mV{\cdot}s^{-1}$) (**C**), Ip (µA) vs υ ($m{\cdot}s.^{-1}$) (**D**)

Selectivity

By applying the mismatch DNA sequences, the selectivity of the sensing assay has been evaluated. The ss-tDNA of 1, 2, and 3 mismatch sequences have been cast on the modified electrode surface and incubated at 37 °C for investigating the selectivity of the engineered bio-assay. Table 1 is used to observe the associated mismatch sequences. For discriminating the identical sequences of different ss-tDNAs, the intended genosensor selectivity has been investigated using the DPV approach. According to Fig. 8A and B, the achieved peak current can be lower than other incompatible sequences because of the effective hybridization of the presented ss-tDNA. Furthermore, compared to the sequence of mismatch targets, the obtained results approve the greater selectivity of the presented platform to distinguish the principal ss-tDNA hybridization. Somehow, the mismatch 1 electrochemical signal is smaller than other mismatches and nearer to the analytical signal of the developed platform for the target gene. It can be the reason for having similarity between the sequence of this mismatch and the sequence of associated *H. influenzae*. However, in the mismatch sequences of 2 and 3, electrochemical signals have been increased because of the aforementioned fact.

Negative control investigation

A negative control has also been studied to approve the selectivity of our new genosensor. For attaining this goal, different bacterial species such as S*almonella typhimurium* and *Shigella dysenteriae* bacteria have been utilized for processing hybridization rather than *Haemophilus influenzae* ss-tDNA. According to Fig. 8C, the peak current obtained for the *H. influenzae sequence* ss-tDNA is lower than the mentioned bacterial sequences regarding their DPV responses. It is considered another confirmation, which validates the greater selectivity of the proposed assay for *H. influenzae*.

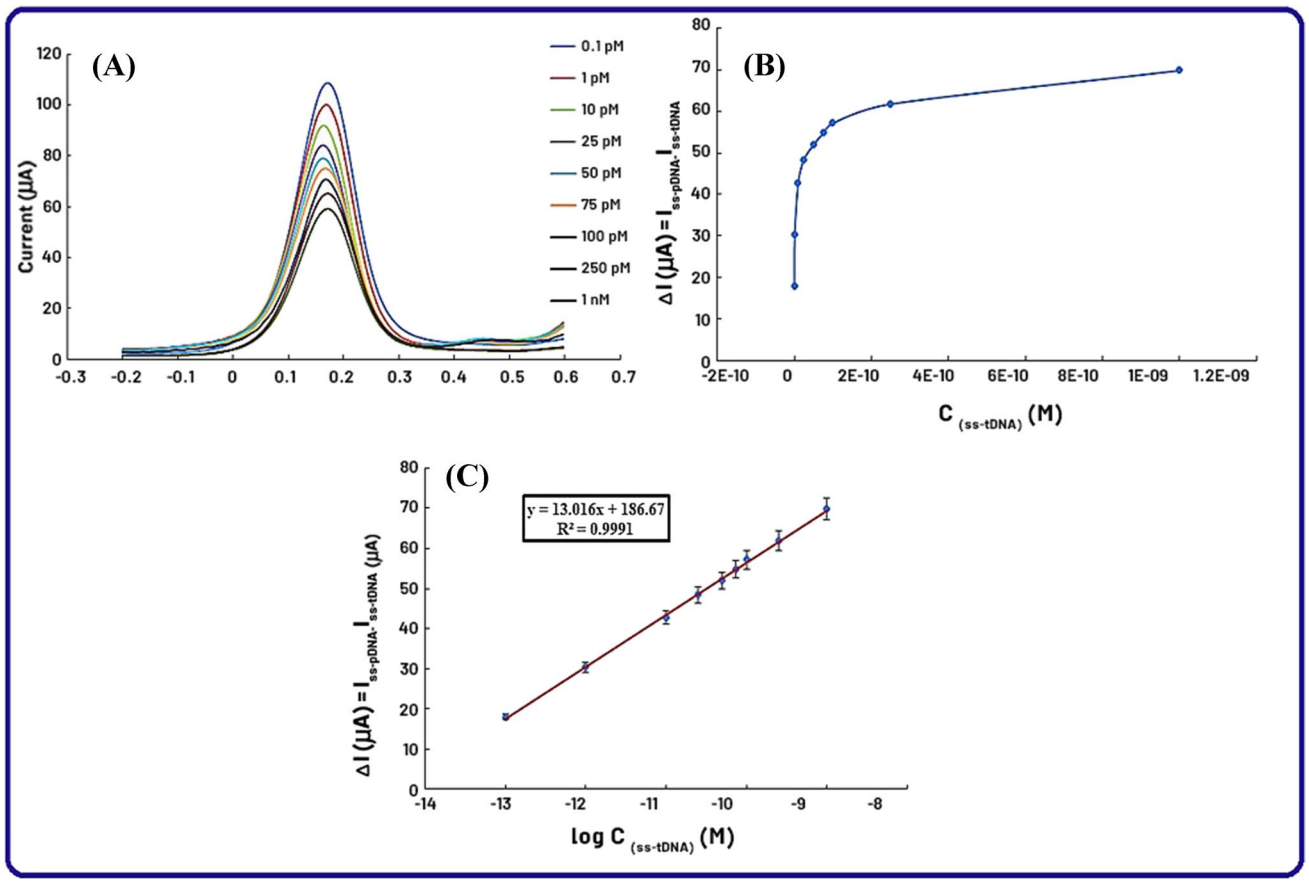

Fig. 7 Voltammograms of the designed bio-assay in various concentrations of the target DNA include 10^{-13}–10^{-9} M with 10^{-1} intervals (**A**). Dependency of peak currents to various concentrations of the target DNA (**B**). Linear calibration plot (logarithmic dependency of peak currents regarding different concentrations of the target DNA of *H. influenzae*) (**C**). E initial = −0.2 V, E end = 0.6 V, equilibration time = 0, Estep = 0.4974 V, frequency = 10 Hz. The error bars represent the standard deviation of five repeats for each measurement

Table 1 Oligonucleotide sequences of *H. influenzae* including ss-pDNA, ss-tDNA, mismatch 1, 2, 3), *Salmonella typhimurium*, and *Shigella flexneri*

	Sequences	Oligonucleotide
1	5'-SH-$(CH_3)_6$ AAT TTT CCA ACT TTT TCA CCT GCA T-5'	*L-fuculokinase* ss-pDNA sequence
2	5'-ATG CAG GTG AAA AAG TTG GAA AAT T-5'	ss-tDNA sequence
3	5'-ATG GAG GTG AAA AAG TTG GAA AAT T-5'	Mismatch 1
4	5'-AGG GAG GTG AAA AAG TTG GAA AAT T-5'	Mismatch 2
5	5'-AGG GAG GTG AGA AAG TTG GAA AAT T-5'	Mismatch 3
6	5'-CAGCCTGTTAAATGCCCTG-5'	*Shigella flexneri* ss-tDNA (uidA β-gulucronidase)
7	5'-CCT CGC AAA TCC GCA TCT TCA TGA C-3'	*Salmonella typhimurium* ss-tDNA (ViaB)

Stability, reproducibility, and repeatability

The performance of the electrochemical reactions in the introduced new genosensor is considered a vital role in the modified electrode stability (NiCr/BC LDH incorporated with AuNPs). The investigation of DPV responses in a solution with $[Fe(CN)_6]^{3-/4-}$ (0.01 M), in the company of KCl for 13 days, is used to assess the stability based on the aforementioned modifier. The obtained voltammograms of the constructed bio-assay confirm the lack of observation among the 13 days by the significant alteration and the electrochemical capability of the genosensing assay is kept via an 88.85% initial response value (Fig. 9A and B).

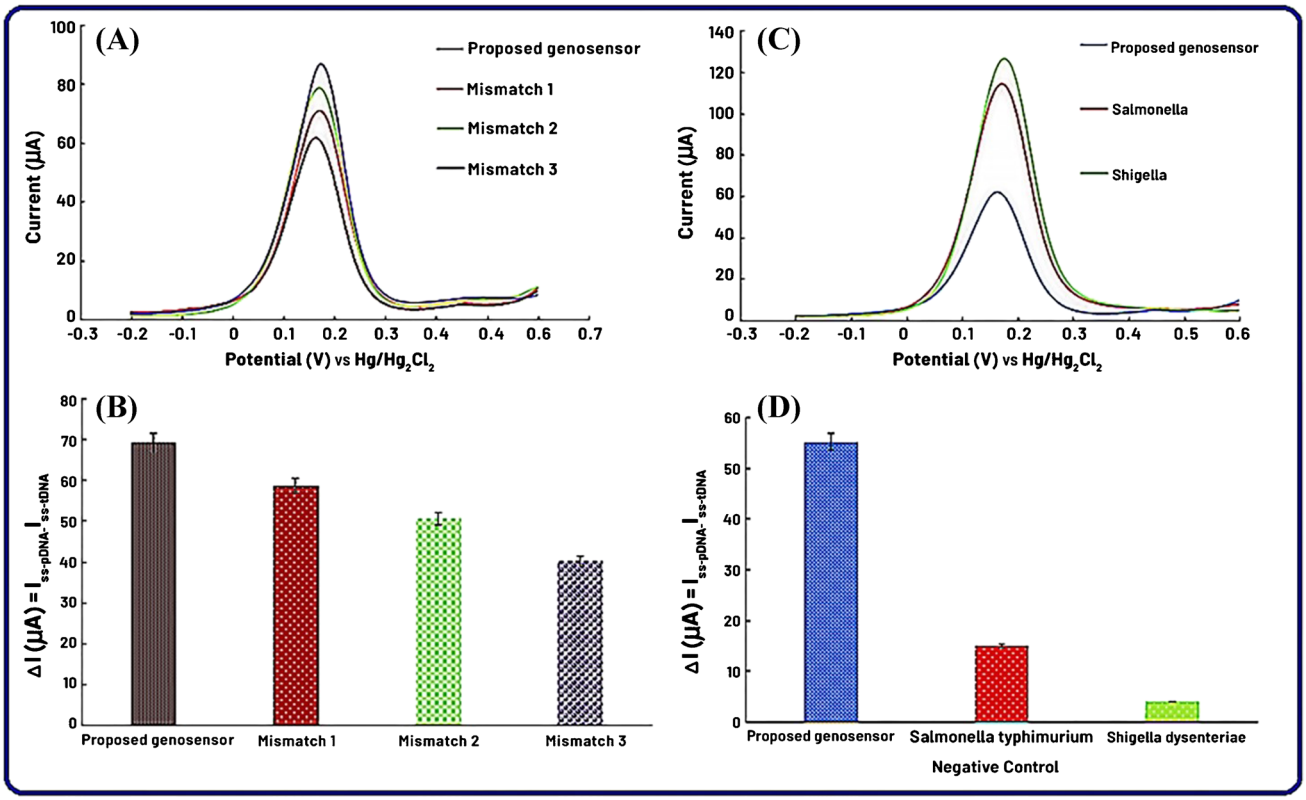

Fig. 8 Selectivity of the fabricated genosensor. DPVs of the fabricated gen detection assay in hybridization by ss-tDNA, 1-mismatch DNA, 2-mismatch, and 3-mismatch DNA (**A**). The scan rate is 50 mV/s. Related histogram demonstrates the proposed genosensing assay selectivity (**B**). DPV voltammograms of negative control of the proposed gene detection assay (**C**). Histogram of the negative control investigation step (**D**)

On the other hand, the CV technique is used to verify the cyclic stability of the fabricated bio-assay. Different cycles such as 1, 5, 10, 20, 40, 60, 80, and 100 are used to perform this step. According to Fig. 9C, it does no clear alteration between the first and the 100th cycles. In another word, the verified cycles are approximately constant. The achieved consequences represent that the label-free assays include a sufficient level of inter- and intraday stability.

Additionally, for considering the reproducibility of the bio-assay, 5 individual electrodes were modified by the prepared nano-biocomposite for determining 1 pM of the associated ss-tDNA, and ultimately, the electrochemical signal was effectively estimated. The RSD of 5 modified electrodes was equal to 2.6%.

Furthermore, five determinations of 1 pM ss-tDNA, as well as one modified electrode (NiCr/BC LDH incorporated with AuNPs), are applied to investigate the repeatability and RSD was equal to 3.2%. Adequate RSDs value for the proposed analytical sensing platform for reproducibility and repeatability steps confirmed good performance and the applicability of the designed genosensor in various biological samples.

The performance of the designed genosensor in urine samples

Spiking various *H. influenzae* ss-tDNA concentrations in urine samples is used to examine the applicability of the designed gene-detection platform in biological samples. The urine sample of a healthy person is freshly collected, and separated from the proteins and salts deposited at the bottom of the centrifuge tube by centrifugation for 20 min at 10,000 rpm. It was then diluted 10 times with the desired buffer without any additional pretreatment and used in voltammetric experiments.

To approve the better performance of the offered gene detection assay, the mixtures of the ss-tDNA 1:1 (v/v) and urine sample have been cast on the modified electrode surface. Then, for determining *H. influenzae* at different ss-tDNA concentrations, DPV measurements have been performed. When the DPV approach is used, the same as the calibration plot in the absence of urine samples, 1 to 1000 pM was obtained for the LR of urine samples without any pretreatment. Additionally, 0.9986 was obtained for the R^2. It was possible to plot the accepting calibration plot for urine samples and the LR of the applied technique has been

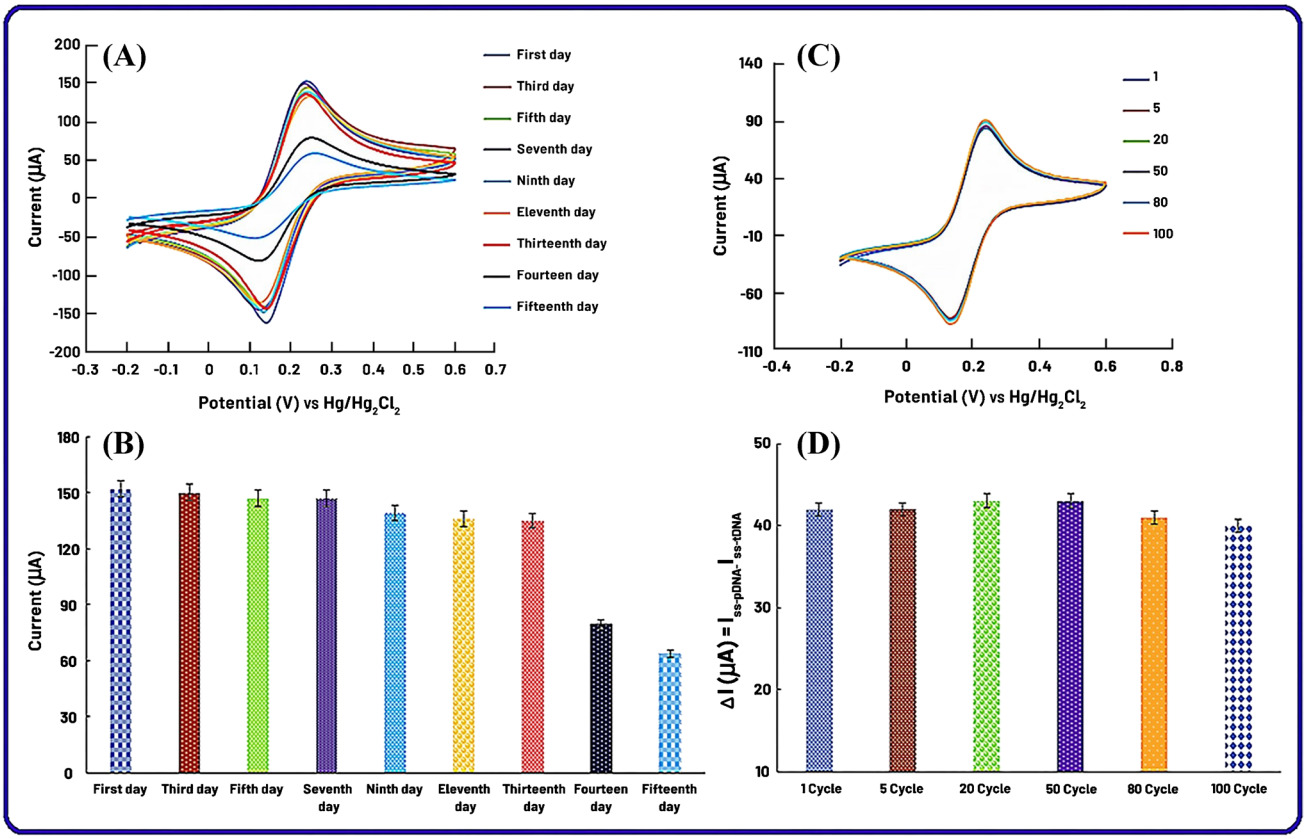

Fig. 9 The investigation of the stability related to the prepared nanocomposite stabilized on the Au electrode in 15 days (**A**). Histogram of the different days demonstrating the stability of the offered sensing assay (**B**). Voltammograms of the LDH/BC/AuNP nanocomposite immobilized on the surface of the Au electrode in various cycle numbers (**C**). Histogram representing the various cycle numbers (**D**)

unchanged with less than 5% differences. Such a fact confirms that no significant impact is provided on the electrochemical signal by the matrix of the urine samples.

On another hand, for estimating the feasible accuracy of the presented genosensor and for examining the effect of the matrix, the DPV in the prepared urine samples is used to study the recovery indexes. To getting such an objective, 4 various *H. influenzae* ss-tDNA concentrations have been added to the different urine samples. Table 2 represents the obtained results. The values of 96.6–104% and 2.3–3.4% were obtained for the recovery indexes and associated RSDs, respectively. This represents that the developed biosensor can be used for the determination of the different pathogenic agents in biological samples with acceptable accuracy.

Comparison of the designed genosensing platform with other assays

Compared to the former clinical methods and developed sensing and biosensing assay, the obtained LOD and LOQ are very small which brings great sensitivity to the engineered gene detection assay because of using BC decorated with the NiCr LDH sheets incorporated with AuNPs stabilized on an Au electrode. A suitable sensing method to determine the *H. influenzae* at low concentrations with an extensive LR represented by the proposed genosensor is demonstrated by the achieved analytical efficiency. Such a situation can be attributed to good electron transport by the developed nanocomposite, the high surface of the modified electrode to immobilization of the DNA, and the great electrical conductivity. Table 3 demonstrates the high applicability of the designed genosensor in comparison with similar research works in this regard.

Conclusion and future perspectives

For detecting *H. influenzae* based on the DPV method, a signal-amplification genosensing-based assay has effectively been fabricated and a high sensitivity has been represented. The detection performance can be improved by three sensor components: First, for enhancing the stability and conductivity, the NiCr LDH/BC application as the electrode modifier agent was helpful. Second, employing AuNPs could be a

Table 2 The electrochemical performance of the designed platform in various urine samples for highly sensitive detection of *H. influenzae* ($n=5$)

Urine samples	C (Added)/pM	C (Found)/pM	Recovery index (%)	Confidence level	RSD (%), $n=5$
1	5	4.83	96.6	±0.029	2.7
2	10	9.88	98.8	±0.033	2.3
3	15	15.7	104	±0.046	3.4
4	20	19.8	99.1	±0.034	2.9

well-qualified signal amplifier. Most of all, strong coordination between thiolated DNA and AuNPs through SAM bounds is used to steadily immobilize more ss-pDNA. This provides stable electrochemical performance and low LOD. Then, high specificity and affinity can be afforded for *H. influenzae*. Third, to lower LOD, the competitive strategy was beneficial. All employed compounds have been utilized for enhancing the surface and increasing the electrochemical signal and afterward, expanding the electron transfer rate. According to mentioned characteristics, *H. influenzae* can be detected to be 6.14 fM with better sensitivity by the assay. The assay can also be used for the detection of the real sample, which suggests expected employment potentiality infeasible applications. According to the achieved outcomes, it has been confirmed that the sensitive bio-assay has the potential for being preferably utilized to detect pathogenic bacteria, especially in real samples like samples of urine. Compared to the previous platforms, such a method can assure a quicker and simpler DNA-based genosensor to distinguish *H. influenzae*. This genosensing bio-assay will also confirm an outstanding potential to select ss-tDNA from 1-, 2-, and 3-base mismatched sequences. In addition, our study demonstrates a discerning sensing device for sensitive recognizing and quantifying *H. influenzae* in counter with negative control. Additionally, it was possible to test the well-fabricated platform for reusability and regeneration steps. Two additional encouraging features of formed genosensor can be considered as the unique characteristics of on-time administration of effective treatment to patients and identifying the infectious agent. Simultaneously, the current study demonstrates the capability of genosensors for being used in the recognition of pathogenic bacteria and can be considered a new method for presenting strong devices for the recognition of substantial pathogens.

Acknowledgements The authors wish to thank the financial support from the University of Tabriz, Tabriz, Iran. The authors are also very much grateful for financial support from the Immunology Research Center, Tabriz University of Medical Sciences.

Funding The authors received financial support from the University of Tabriz, Tabriz, Iran, and from the Immunology Research Center, Tabriz University of Medical Sciences.

Data availability The datasets generated during and/or analysed during the current study are available from the corresponding author on reasonable request.

Declarations

Conflict of interest The authors declare no competing interests.

References

1. Sohrabi H, Majidi MR, Nami F, Asadpour-Zeynali K, Khataee A, Mokhtarzadeh A (2021) A novel engineered label-free Zn-based MOF/CMC/AuNPs electrochemical genosensor for highly sensitive determination of Haemophilus influenzae in human plasma samples. Microchim Acta 188(3):1–16
2. Mobed A, Baradaran B, de la Guardia M, Agazadeh M, Hasanzadeh M, Rezaee MA, Mosafer J, Mokhtarzadeh A, Hamblin MR (2019) Advances in detection of fastidious bacteria: from

Table 3 The comparison of the designed genosensing bio-assay based on LDH/BC/AuNP–modified Au electrode with other related analytical and clinical methods for highly sensitive recognition of *H. influenzae*

Recognition method	Modifier agents	LOD	Linear range	Reference
Electrochemical genosensor	Zn-based MOF/CMC/AuNPs	1.48 fM	0.1 pM–10 nM	[1]
Plasmonic contrast imaging biosensor	–	8.6 nM	–	[69]
Aptamer assay	Poly-(4-amino-3-hydroxynapthalene sulfonic acid) (p-AHNSA)	0.02 nM	0.1–2500 nM	[70]
Aptamer-functionalized field-effect transistor (FET)	–	5.9 pM	10 pM to 10 nM	[71]
Duplex quantitative PCR	–	0.0125 pM	–	[72]
Immunochromatographic strip	Gold	–	–	[73]
DNA-based genosensing assay	NiCr LDH/BC/AuNPs	6.14 fM	0.1–1000 pM	Present study

microscopic observation to molecular biosensors. TrAC Trends Anal Chem 113:157–171
3. Özyurt C, Uludağ İ, İnce B, Sezgintürk MK (2021) Biosensing strategies for diagnosis of prostate specific antigen. J Pharm Biomed Anal 209:114535
4. Karaboğa MNS, Sezgintürk MK (2022) Biosensor approaches on the diagnosis of neurodegenerative diseases: sensing the past to the future. J Pharm Biomed Anal 209:114479
5. Zanella M-C, Cherkaoui A, Hinic V, Renzi G, Goldenberger D, Egli A, Schrenzel J (2021) Unexpectedly high false-positive rates for Haemophilus influenzae using a meningoencephalitis syndromic PCR panel in two tertiary centers. Front Cell Infect Microbiol 11:120
6. Cheng X, Zheng S, Wang W, Han H, Yang X, Shen W, Wang C, Wang S (2021) Synthesis of two-dimensional graphene oxide-fluorescent nanoprobe for ultrasensitive and multiplex immunochromatographic detection of respiratory bacteria. Chem Eng J 426:131836
7. Sawada T, Katayama M, Takatani S, Ohiro Y (2021) Early detection of drug-resistant Streptococcus pneumoniae and Haemophilus influenzae by quantitative flow cytometry. Sci Rep 11(1):1–8
8. Pei L, Zhang S, Huang L, Geng X, Ma L, Jiang W, Li W, Chen D (2020) Antiviral agents, glucocorticoids, antibiotics, and intravenous immunoglobulin usage in 1142 patients with coronavirus disease 2019: a systematic review and meta-analysis. Pol Arch Intern Med 130(9):726–733
9. Roushdy C, Moustafa A, Abdelwahab M, Ibrahim F, El-bauomy E (2021) Latex agglutination: a rapid, specific immunoassay for diagnosis of ruminant brucellosis. Adv Anim Vet Sci 9(9):1292–1301
10. Rostami S, Moeineddini L, Ghandehari F, Khorasani MR, Shoaei P, Ebrahimi N (2021) Macrolide-resistance, capsular genotyping and associated factors of group B Streptococci colonized pregnant women in Isfahan, Iran. Iran J Microbiol 13(2):183–189
11. Şenocak A, Tümay SO, Ömeroğlu İ, Şanko V (2022) Crosslinker polycarbazole supported magnetite MOF@ CNT hybrid material for synergetic and selective voltammetric determination of adenine and guanine. J Electroanal Chem 905:115963
12. Sanko V, Şenocak A, Oğuz Tümay S, Çamurcu T, Demirbas E (2022) Core-shell hierarchical enzymatic biosensor based on hyaluronic acid capped copper ferrite nanoparticles for determination of endocrine-disrupting bisphenol A. Electroanalysis 34(3):561–572
13. Eivazzadeh-Keihan R, Pashazadeh-Panahi P, Baradaran B, de la Guardia M, Hejazi M, Sohrabi H, Mokhtarzadeh A, Maleki A (2018) Recent progress in optical and electrochemical biosensors for sensing of Clostridium botulinum neurotoxin. TrAC Trends Anal Chem 103:184–197
14. Manring N, Ahmed MM, Tenhoff N, Smeltz JL, Pathirathna P (2022) Recent advances in electrochemical tools for virus detection. Anal Chem 94(20):7149–7157
15. Hasanzadeh M, Karimzadeh A, Sadeghi S, Mokhtarzadeh A, Shadjou N, Jouyban A (2016) Graphene quantum dot as an electrically conductive material toward low potential detection: a new platform for interface science. J Mater Sci Mater Electron 27(6):6488–6495
16. Hasanzadeh M, Mokhtarzadeh A, Shadjou N, Mahboob S (2017) An innovative immunosensor for detection of tumor suppressor protein p53 in unprocessed human plasma and cancer cell lysates. Int J Biol Macromol 105:1337–1348
17. Hasanzadeh M, Sadeghi S, Bageri L, Mokhtarzadeh A, Shadjou N, Mahboob S (2016) Poly-dopamine-beta-cyclodextrin: a novel nanobiopolymer towards sensing of some amino acids at physiological pH. Mater Sci Eng C 69:343–357
18. Safarpour H, Dehghani S, Nosrati R, Zebardast N, Alibolandi M, Mokhtarzadeh A, Ramezani M (2020) Optical and electrochemical-based nano-aptasensing approaches for the detection of circulating tumor cells (CTCs). Biosens Bioelectron 148:111833
19. Sohrabi H, Khataee A, Ghasemzadeh S, Majidi MR, Orooji Y (2021) Layer double hydroxides (LDHs)-based electrochemical and optical sensing assessments for quantification and identification of heavy metals in water and environment samples: a review of status and prospects Trends Environ Anal Chem 31:e00139
20. Mobed A, Nami F, Hasanzadeh M, Hassanpour S, Saadati A, Mokhtarzadeh A (2019) A novel nucleic acid based bio-assay toward recognition of Haemophilus influenza using bioconjugation and DNA hybridization method. Int J Biol Macromol 139:1239–1251
21. Sohrabi H, Majidi MR, Fakhraei M, Jahanban-Esfahlan A, Hejazi M, Oroojalian F, Baradaran B, Tohidast M, de la Guardia M, Mokhtarzadeh A (2022) Lateral flow assays (LFA) for detection of pathogenic bacteria: a small point-of-care platform for diagnosis of human infectious diseases. Talanta 243:123330
22. Tümay SO, Şenocak A, Sarı E, Şanko V, Durmuş M, Demirbas E (2021) A new perspective for electrochemical determination of parathion and chlorantraniliprole pesticides via carbon nanotube-based thiophene-ferrocene appended hybrid nanosensor. Sens Actuators B Chem 345:130344
23. Orooji Y, Sohrabi H, Hemmat N, Oroojalian F, Baradaran B, Mokhtarzadeh A, Mohaghegh M, Karimi-Maleh H (2021) An overview on SARS-CoV-2 (COVID-19) and other human coronaviruses and their detection capability via amplification assay, chemical sensing, biosensing, immunosensing, and clinical assays. Nanomicro Lett 13(1):1–30
24. Sohrabi H, Arbabzadeh O, Khaaki P, Khataee A, Majidi MR, Orooji Y (2021) Patulin and Trichothecene: characteristics, occurrence, toxic effects and detection capabilities via clinical, analytical and nanostructured electrochemical sensing/biosensing assays in foodstuffs. Crit Rev Food Sci Nutr 62(20):5540–5568
25. Sadeghi P, Sohrabi H, Hejazi M, Jahanban-Esfahlan A, Baradaran B, Tohidast M, Majidi MR, Mokhtarzadeh A, Tavangar SM, de la Guardia M (2021) Lateral flow assays (LFA) as an alternative medical diagnosis method for detection of virus species: the intertwine of nanotechnology with sensing strategies. TrAC Trends Anal Chem 145:116460
26. Sohrabi H, Bolandi N, Hemmati A, Eyvazi S, Ghasemzadeh S, Baradaran B, Oroojalian F, Majidi MR, de la Guardia M, Mokhtarzadeh A (2022) State-of-the-art cancer biomarker detection by portable (Bio) sensing technology: a critical review. Microchem J 177:107248
27. Kucherenko I, Soldatkin O, Dzyadevych S, Soldatkin A (2020) Electrochemical biosensors based on multienzyme systems: main groups, advantages and limitations–a review. Anal Chim Acta 1111:114–131
28. Flauzino JM, Nguyen EP, Yang Q, Rosati G, Panáček D, Brito-Madurro AG, Madurro JM, Bakandritsos A, Otyepka M, Merkoçi A (2022) Label-free and reagentless electrochemical genosensor based on graphene acid for meat adulteration detection. Biosens Bioelectron 195:113628
29. Sohrabi H, Hemmati A, Majidi MR, Eyvazi S, Jahanban-Esfahlan A, Baradaran B, Adlpour-Azar R, Mokhtarzadeh A, de la Guardia M (2021) Recent advances on portable sensing and biosensing assays applied for detection of main chemical and biological pollutant agents in water samples: a critical review. TrAC Trends Anal Chem 143:116344
30. Sohrabi H, Javanbakht S, Oroojalian F, Rouhani F, Hanifehpour Y, Hashemzaei M, Shaabani A, Mokhtarzadeh A, Morsali A (2021) Nanoscale metal-organic frameworks: recent developments in synthesis, modifications and bioimaging applications. Chemosphere 281:130717

31. Sohrabi H, Majidi MR, Arbabzadeh O, Khaaki P, Pourmohammad S, Khataee A, Orooji Y (2022) Recent advances in the highly sensitive determination of zearalenone residues in water and environmental resources with electrochemical biosensors. Environ Res 204:112082
32. Djebbi K, Xing J, Weng T, Bahri M, Elaguech MA, Du C, Shi B, Hu L, He S, Liao P (2022) Highly sensitive fluorescence multiplexed miRNAs biosensors for accurate clinically diagnosis lung cancer disease using LNA-modified DNA probe and DSN enzyme. Anal Chim Acta 1208:339778
33. Sohrabi H, Majidi MR, Asadpour-Zeynali K, Khataee A, Mokhtarzadeh A (2022) Bimetallic Fe/Mn MOFs/MβCD/AuNPs stabilized on MWCNTs for developing a label-free DNA-based genosensing bio-assay applied in the determination of Salmonella typhimurium in milk samples. Chemosphere 287:132373
34. Soozanipour A, Sohrabi H, Abazar F, Khataee A, Noorbakhsh A, Asadnia M, Taheri-Kafrani A, Majidi MR, Razmjou A (2021) Ion selective nanochannels: from critical principles to sensing and biosensing applications. Adv Mater Technol 6(10):2000765
35. Sohrabi H, kholafazad Kordasht H, Pashazadeh-Panahi P, Nezhad-Mokhtari P, Hashemzaei M, Majidi MR, Mosafer J, Oroojalian F, Mokhtarzadeh A, de la Guardia M (2020) Recent advances of electrochemical and optical biosensors for detection of C-reactive protein as a major inflammatory biomarker Microchem J 158:105287
36. Jalili R, Khataee A, Rashidi M-R, Razmjou A (2020) Detection of penicillin G residues in milk based on dual-emission carbon dots and molecularly imprinted polymers. Food Chem 314:126172
37. Şenocak A, Tümay SO, Sarı E, Şanko V, Durmuş M, Demirbas E (2021) The simultaneously voltammetric determination of spinosad and chlorantraniliprole pesticides by carbazole-ferrocene functionalized carbon nanotube architecture. J Electrochem Soc 168(8):087513
38. Yeh S-H, Huang M-S, Huang C-H (2022) Electrochemical sensors for sulfamethoxazole detection based on graphene oxide/graphene layered composite on indium tin oxide substrate. J Taiwan Inst Chem Eng 131:104155
39. Arshad MM, Gopinath SC, Ibau C, Nuzaihan M, Fathil M, Azmi UM, Anbu P (2022) Faradaic electrochemical impedimetric analysis on MoS2/Au-NPs decorated surface for C-reactive protein detection. J Taiwan Inst Chem Eng 138:104450
40. Mei Y, He C, Zeng W, Luo Y, Liu C, Yang M, Kuang Y, Lin X, Huang Q (2022) Electrochemical biosensors for foodborne pathogens detection based on carbon nanomaterials: recent advances and challenges. Food Bioprocess Technol 15:498–513
41. Idili A, Parolo C, Alvarez-Diduk R, Merkoçi A (2021) Rapid and efficient detection of the SARS-CoV-2 spike protein using an electrochemical aptamer-based sensor. ACS Sens 6(8):3093–3101
42. Sohrabi H, Majidi MR, Asadpour-Zeynali K, Khataee A, Dastborhan M, Mokhtarzadeh A (2021) A PCR-free genosensing platform for detection of Shigella dysenteriae in human plasma samples by porous and honeycomb-like biochar decorated with ultrathin flower-like MoS2 nanosheets incorporated with Au nanoparticles. Chemosphere 288:132531
43. Sohrabi H, Majidi MR, Khaki P, Jahanban-Esfahlan A, de la Guardia M, Mokhtarzadeh A (2022) State of the art: lateral flow assays toward the point-of-care foodborne pathogenic bacteria detection in food samples. Comp Rev Food Sci Food Safe 21(2):1868–1912
44. Negahdary M, Sattarahmady N, Heli H (2020) Advances in prostate specific antigen biosensors-impact of nanotechnology. Clin Chim Acta 504:43–55
45. Rajkumar C, Kim H (2022) Interface engineering of ruthenium-supported sulfur-doped graphitic carbon nitride for ultrasensitive electrochemical determination of riboflavin. J Taiwan Inst Chem Eng 138:104470
46. Idili A, Bonini A, Parolo C, Alvarez-Diduk R, Di Francesco F, Merkoçi A (2022) A programmable electrochemical Y-shaped DNA scaffold sensor for the single-step detection of antibodies and proteins in untreated biological fluids. Adv Func Mater 32(37):2201881
47. Huang Q, Lin X, Zhu J-J, Tong Q-X (2017) Pd-Au@ carbon dots nanocomposite: Facile synthesis and application as an ultrasensitive electrochemical biosensor for determination of colitoxin DNA in human serum. Biosens Bioelectron 94:507–512
48. de Eguilaz MR, Cumba LR, Forster RJ (2020) Electrochemical detection of viruses and antibodies: a mini review. Electrochem Commun 116:106762
49 Majidi MR, Sohrabi H (2022) Chiral conductive polymers, conductive polymers in analytical chemistry. ACS Publications, Washington, DC, pp 287–312
50. Farhat H, Célier J, Forano C, Mousty C (2021) Evaluation of hierarchical glucose oxidase/Co3Mn-CO3 LDH modified electrodes for glucose detection. Electrochim Acta 376:138050
51. Baig N, Sajid M (2017) Applications of layered double hydroxides based electrochemical sensors for determination of environmental pollutants: a review. Trends Environ Anal Chem 16:1–15
52. Mirzaee MT, Seidi S, Alizadeh R (2021) Pipette-tip SPE based on Graphene/ZnCr LDH for Pb (II) analysis in hair samples followed by GFAAS. Anal Biochem 612:113949
53. Soltani R, Marjani A, Shirazian S (2020) A hierarchical LDH/MOF nanocomposite: single, simultaneous and consecutive adsorption of a reactive dye and Cr (vi). Dalton Trans 49(16):5323–5335
54. Sohrabnezhad S, Poursafar Z, Asadollahi A (2020) Synthesis of novel core@ shell of MgAl layered double hydroxide@ porous magnetic shell (MgAl-LDH@ PMN) as carrier for ciprofloxacin drug. Appl Clay Sci 190:105586
55. Wu K, Xu S, Tian X-Y, Zeng H-Y, Hu J, Guo Y-H, Jian J (2021) Renewable lignin-based surfactant modified layered double hydroxide and its application in polypropylene as flame retardant and smoke suppression. Int J Biol Macromol 178:580–590
56. Kubo D, Tadanaga K, Hayashi A, Tatsumisago M (2020) Fabrication of Mg-Al layered double hydroxide thin membrane for all-solid-state alkaline fuel cell using glass paper as a support. Front Mater 7:117
57. Tao Y, Lao Y-H, Yi K, Xu Y, Wang H, Shao D, Wang J, Li M (2021) Noble metal-molybdenum disulfide nanohybrids as dual fluorometric and colorimetric sensor for hepatitis B virus DNA detection. Talanta 234:122675
58. Taherian Z, Khataee A, Orooji Y (2020) Facile synthesis of yttria-promoted nickel catalysts supported on MgO-MCM-41 for syngas production from greenhouse gases. Renew Sustain Energy Rev 134:110130
59. Moradi M, Vasseghian Y, Khataee A, Harati M, Arfaeinia H (2021) Ultrasound-assisted synthesis of FeTiO3/GO nanocomposite for photocatalytic degradation of phenol under visible light irradiation. Sep Purif Technol 261:118274
60. Kalinke C, de Oliveira PR, Bonacin JA, Janegitz BC, Mangrich A, Júnior LHM, Bergamini M (2021) State-of-art and perspectives in the use of biochar for electrochemical and electroanalytical applications. Green Chem 23:5272–5301
61. Huang Q, Lin X, Chen D, Tong Q-X (2022) Carbon Dots/α-Fe2O3-Fe3O4 nanocomposite: efficient synthesis and application as a novel electrochemical aptasensor for the ultrasensitive determination of aflatoxin B1. Food Chem 373:131415
62. Merkoçi A, Pumera M, Llopis X, Pérez B, Del Valle M, Alegret S (2005) New materials for electrochemical sensing VI: carbon nanotubes. TrAC Trends Anal Chem 24(9):826–838
63. Hasanzadeh M, Tagi S, Solhi E, Shadjou N, Jouyban A, Mokhtarzadeh A (2018) Immunosensing of breast cancer prognostic marker in adenocarcinoma cell lysates and unprocessed human

plasma samples using gold nanostructure coated on organic substrate. Int J Biol Macromol 118:1082–1089
64. Hasanzadeh M, Baghban HN, Shadjou N, Mokhtarzadeh A (2018) Ultrasensitive electrochemical immunosensing of tumor suppressor protein p53 in unprocessed human plasma and cell lysates using a novel nanocomposite based on poly-cysteine/graphene quantum dots/gold nanoparticle. Int J Biol Macromol 107:1348–1363
65. Chen Z, Deng H, Zhang M, Yang Z, Hu D, Wang Y, Yan K (2020) One-step facile synthesis of nickel–chromium layered double hydroxide nanoflakes for high-performance supercapacitors. Nanoscale Adv 2(5):2099–2105
66. Xia S, Dai T, Meng Y, Zhou X, Pan G, Zhang X, Ni Z (2020) A low-temperature water–gas shift reaction catalyzed by hybrid NiO@ NiCr-layered double hydroxides: catalytic property, kinetics and mechanism investigation. Phys Chem Chem Phys 22(22):12630–12643
67. Sohrabi H, Majidi MR, Asadpour-Zeynali K, Khataee A, Dastborhan M, Mokhtarzadeh A (2022) A PCR-free genosensing platform for detection of Shigella dysenteriae in human plasma samples by porous and honeycomb-like biochar decorated with ultrathin flower-like MoS2 nanosheets incorporated with Au nanoparticles. Chemosphere 288:132531
68. Ikken Y, Benaouda A, Yaich LI, Hilali F, Sekhsokh Y, Charof R (2021) Simultaneous detection of Neisseria meningitidis, Streptococcus pneumoniae and Haemophilus influenzae by quantitative PCR from CSF samples with negative culture in Morocco. Acta Microbiologica et Immunologica Hungarica 68(2):107–112
69. Wong CL, Chan JY, Choo LX, Lim HQ, Mittman H, Olivo M (2019) Plasmonic contrast imaging biosensor for the detection of H3N2 influenza protein-antibody and DNA-DNA molecular binding. IEEE Sens J 19(24):11828–11833
70. Yadav SK, Agrawal B, Chandra P, Goyal RN (2014) Bioelectronics, In vitro chloramphenicol detection in a Haemophilus influenza model using an aptamer-polymer based electrochemical biosensor. Biosens Bioelectron 55:337–342
71. Kwon J, Lee Y, Lee T, Ahn J-H (2020) Aptamer-based field-effect transistor for detection of avian influenza virus in chicken serum. Anal Chem 92(7):5524–5531
72. De Gier C, Pickering JL, Richmond PC, Thornton RB, Kirkham L-AS (2016) Duplex quantitative PCR assay for detection of Haemophilus influenzae that distinguishes fucose-and protein D-negative strains. J Clin Microbiol 54(9):2380–2383
73. Tao Y, Hao H, Li J, Wang M, Wang Y, Zhang G, Hu Z (2019) Colloidal gold immunochromatographic strip for rapid detection of Haemophilus influenzae. Chin J Biotechnol 35(5):901–909